



**HAL**  
open science

# Lattice friction for crystalline defects: from dislocations to cracks

Olga Kresse, Lev Truskinovsky

► **To cite this version:**

Olga Kresse, Lev Truskinovsky. Lattice friction for crystalline defects: from dislocations to cracks. Journal of the Mechanics and Physics of Solids, 2004, 52, pp.2521-2543. 10.1016/j.jmps.2004.04.011 . hal-00111405

**HAL Id: hal-00111405**

**<https://hal.science/hal-00111405v1>**

Submitted on 9 Jul 2019

**HAL** is a multi-disciplinary open access archive for the deposit and dissemination of scientific research documents, whether they are published or not. The documents may come from teaching and research institutions in France or abroad, or from public or private research centers.

L'archive ouverte pluridisciplinaire **HAL**, est destinée au dépôt et à la diffusion de documents scientifiques de niveau recherche, publiés ou non, émanant des établissements d'enseignement et de recherche français ou étrangers, des laboratoires publics ou privés.

# Lattice friction for crystalline defects: from dislocations to cracks

O. Kresse<sup>a</sup>, L. Truskinovsky<sup>b,\*</sup>

<sup>a</sup>*Department of Aerospace Engineering and Mechanics, University of Minnesota, 110 Union Street, 107 Akerman Hall, Minneapolis, MN 55455, USA*

<sup>b</sup>*Laboratoire de Mécanique des Solides, CNRS-UMR 7649, Ecole Polytechnique, Palaiseau 91128, Cedex, France*

---

## Abstract

We propose a discrete model providing a unified description of lattice induced drag for a class of defects which includes martensitic phase boundaries, dislocations and cracks. Although the model is Hamiltonian, it generates a non-trivial macroscopic friction law which we present as a closed form functional relation between the velocity of the defect and the conjugate configurational force. The possibility to obtain an exact analytic solution of the dynamic problem allows us to expose both the similarities and the differences in the kinetics of various types of defects. In particular, we trace the origin of the symmetry related resonances, specific for dislocations, and show how the flattening of one of the energy wells, indicating transition to fracture, generates a morphological instability of the displacement profile at a critical velocity.

*Keywords:* A. Phase transformations; Plasticity; Fracture; B. Dynamics; Lattice models; C. Cracks; Dislocations; Phase boundaries; Defects

---

## 1. Introduction

Some important features of dynamics are common to most crystal defects. Experiment shows that for martensitic phase boundaries, dislocations and cracks the kinetic behavior can be roughly described by a dry friction law: (i) in the absence of thermal

---

\* Corresponding author. Laboratoire de Mécanique des Solides, CNRS-UMR 7649, Ecole Polytechnique, Palaiseau 91128, Cedex, France. Tel.: +33-1-69333344; fax: +33-1-69333026.

*E-mail addresses:* mart0814@umn.edu (O. Kresse), trusk@lms.polytechnique.fr (L. Truskinovsky).

fluctuations a static defect remains pinned till the driving force exceeds the critical threshold which is at least as high as the smallest force required for the propagation of the defect; (ii) slow steady-state regimes appear to be unstable and one typically observes a sharp transition from a “creep” stage, when the defect moves by thermally activated barrier crossing, to fully inertial dynamics; (iii) the fast continuous branch of the force–velocity relation begins at some finite velocity and continues as a monotone function with characteristically weak dependence on force except in the vicinity of the sonic speed (e.g. Johnston and Gilman, 1959; Nishiyama, 1978; Alshits and Indenbom, 1986; Freund, 1990; Hirth and Lothe, 1972; Abeyaratne and Knowles, 1997; Fineberg and Marder, 1999). This behavior is quite different from the prediction of the elasticity theory where the singularities of elastic fields, representing crystal defects, can move freely without friction. The problem arises because the continuum theory fails to describe processes in the core of a defect if its width is of the order of several lattice spacings.

The fact that a non-zero driving force is required to sustain inelastic deformation, means that the moving defect experiences a non-zero friction; since this effect disappears in the continuum limit, it can be linked to the discreteness of the material. Although there are several physical phenomena contributing to the overall drag force, in this paper we focus on the main low-temperature mechanism associated with radiation drag. It can be understood if we recall that in a lattice the defect moves approximately as a particle placed in a tilted Peierls–Nabarro landscape (Nabarro, 1987). The oscillations of the velocity accompanying such motion create resonances with the short wave spectrum of the lattice, leading to the energy transfer from the moving singularity to the radiation modes. The straightforward macro-description is then incomplete due to the unavoidable energy loss from long to short waves.

The traditional way of dealing with the deficiency of the long wave approximation is to complement continuum model with the phenomenological jump/singularity conditions (kinetic relations) specifying the mechanism of dissipation at small scales. The similarity of the empirical kinetic relations for various types of defects can be linked to the fact that the underlying microscopic phenomenon of successive “breaking” of atomic bonds is always the same. By studying the microscopic features of the steady-state bond breaking process one can therefore assess the mechanism of the intrinsic resistance encountered in fracture, plasticity and pseudo-elasticity of shape memory alloys. The prototypical model, providing a unified description of all these apparently different material phenomena, must contain a possibility of dynamic internal buckling and the simplest elastic coupling between the buckling units making the propagation possible. The fine difference between various defects can then be recovered through particular structure of the energy non-convexity simulating snapping elements.

In what follows we consider a one-parametric family of discrete models of this type allowing one to obtain the macroscopic kinetic relation explicitly. The models are Hamiltonian and the apparent dissipation is due to micro-instabilities and induced radiation of lattice waves carrying energy away from the propagating defect. The mechanical system under consideration may be viewed as a one-dimensional (1D) network of harmonically coupled bi-stable snap-springs (generalized Frenkel–Kontorova (FK) model). Depending on the relative curvatures of the competing energy wells and on

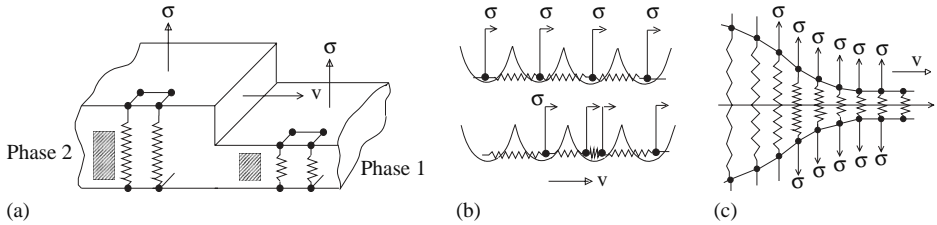


Fig. 1. Schematic configuration of particles around the core of a moving defect: (a) phase boundary, vertical displacements (b) dislocation, horizontal displacements (standard FK model) (c) crack, vertical displacements. Solid links must be interpreted as “shear” springs.

their degree of degeneracy, this model describes a thin film undergoing “thickness” martensitic phase transition, a dislocation or an isolated crack tip (see Fig. 1). The use of the FK model for modelling dislocations is standard (see Braun and Kivshar, 1998); recently it has also been applied to fracture (e.g. Thompson, 1986; Marder and Gross, 1995; Langer, 1992) and martensitic phase transitions (e.g. Kresse and Truskinovsky, 2003). To drive the system off equilibrium we apply to the elements an external distributed force which creates a bias towards one of the energy wells and makes the propagation of a switching wave (kink) energetically favorable. Our goal then is to compute the energy release rate associated with the steady-state motion of the kink and relate it to the velocity through the corresponding friction law (kinetic relation).

In order to obtain an explicit solution for the steady-state problem we follow the work of Weiner (1964), Atkinson and Cabrera (1965), Rogula (1967), Ishioka (1973), Earmme and Weiner (1974,1977), Fath (1988), Kresse and Truskinovsky (2003) and Carpio and Bonilla (2003) among others, and choose the potential of the snap-springs to be two-parabolic. We notice that in all above papers the two “phases” are symmetric with equal elastic moduli. The new element in the present analysis is the *asymmetry* of the energy wells. We preserve the advantage of a fully transparent analytic treatment available for the case of symmetric wells by replacing the direct Fourier transform with the Wiener–Hopf technique. Similar methods have been previously used in discrete piece-wise linear models of 2D fracture Slepyan (1981, 2000, 2001a,b,c, 2002), Marder and Gross (1995), Langer and Lobkovsky (1998), Kessler and Levine (2001) and Pechenik et al. (2002). A direct analysis of the 2D lattice with bi-stable elements covering both dislocations and cracks has been recently done by Slepyan and Ayzenberg-Stepanenko (2004) whose model can be interpreted as a Peierls–Nabarro analog of the present model. The influence of explicit viscous damping at the lattice level on the macroscopic kinetics was studied in both one and two dimensions by Ishioka (1973), Elmer and Van Vleck (1999), Slepyan (2002), Kresse (2002), Carpio and Bonilla (2003) and Slepyan and Ayzenberg-Stepanenko (2004). Other relevant studies of radiative damping associated with phase transitions, plasticity and fracture in discrete systems can be found in Currie et al. (1977), Peyrard and Kruskal (1984), Slepyan and Troyankina (1984), Willis et al. (1986), Kevrekidis and Weinstein (2000),

Cattuno et al. (2001) and references cited therein. Various quasi-continuum approximations going beyond the straightforward continuum elasticity were recently reviewed by Kresse and Truskinovsky (2003).

The main focus of the present paper is the influence of the asymmetry of the energy wells on the kinetic relations. By constructing an exact solution of the general problem with arbitrary degree of asymmetry we create a link between the case of dislocations, where the presence of two equally stiff energy wells essentially control the total displacement discontinuity, with another limiting case when one of the energy wells degenerates. In the latter case the given displacement discontinuity is replaced by the requirement of zero tractions and a dislocation transforms into a crack. Although the overall structure of the kinetic relation in the two limiting cases is quite similar, we observe a considerable restructuring of the displacement profile. Our computations show that while the dislocation profile is “morphologically” stable, the crack profile exhibits a strong parameter sensitivity near a particular value of velocity where it rapidly develops a dendrite-type oscillatory structure. This phenomenon may be related to the well-known branching instability of the dynamic cracks (e.g. Sharon et al., 1995; Marder and Liu, 1993; Gao, 1993).

Contrary to most of the previous studies, we present the ensuing kinetic relation in terms of the velocity dependence of the appropriately chosen configurational force. As we show in a generic bi-linear model, the configurational force is a quadratic function of the applied stress, which reduces to a linear function only in the case of dislocations (Peach–Koehler case). The qualitative comparison of our kinetic relations with experimental data shows that despite its simplicity the proposed discrete model is compatible with dynamic properties of all three mentioned types of defects. The fact that the friction laws appear to be qualitatively similar in fracture, plasticity and pseudo-elasticity of martensitic materials suggests that in all these cases radiative damping plays a dominant role as a low-temperature dissipation mechanism.

The paper is organized as follows. In Section 2 we introduce the piece-wise linear model and formulate the boundary value problem for the traveling waves. In Section 3 we use the Wiener–Hopf technique to solve the discrete problem analytically and to reconstruct the spectrum of excited waves. The displacement profile is then obtained as a superposition of these waves with the proper account of the radiation conditions. In Section 4 by assessing the total energy flux due to the radiated waves at  $\pm$  infinity, we derive the general form of the kinetic relation (friction law) for the configurational force and then specialize it for different types of defects. The last section contains our conclusions. A study of the static case is presented in the Appendix for completeness.

## 2. The model

Consider an array of bi-stable elements coupled through harmonic nearest-neighbor interactions. Denote by  $\tilde{u}_n$  the displacement of the particle with index  $n$  from its reference position and assume that the on-site potential of the bi-stable elements  $w(\tilde{u}_n)$

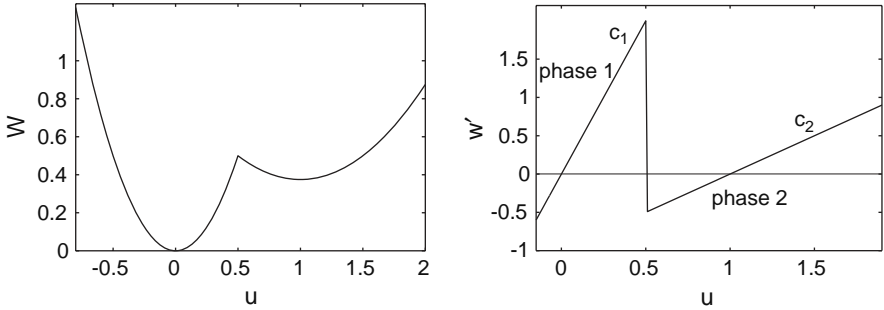


Fig. 2. Bi-quadratic on-site potential and the corresponding force–elongation relation. Parameters:  $a = 1$ ,  $c_1 = 4$ ,  $c_2 = 1$ .

is piece-wise quadratic (see Fig. 2)

$$w(\tilde{u}_n) = \begin{cases} \frac{1}{2} c_1 \tilde{u}_n^2, & \tilde{u}_n < a/2, \\ \frac{1}{2} c_2 (\tilde{u}_n - a)^2 + \frac{a^2}{8} (c_1 - c_2), & \tilde{u}_n > a/2. \end{cases} \quad (1)$$

Suppose that the two energy wells have different curvatures  $c_1 \neq c_2$ . We will refer to the special case when  $c_2 = c_1$ , as a model of a dislocation/twin boundary and to the case when one of the minima is flat, say  $c_2 = 0$ , as corresponding to fracture; the intermediate cases can be associated with martensitic phase transitions (Truskinovsky, 1996).

To bias one of the wells we introduce an external force per unit length  $\tilde{\sigma}$ , acting in the direction of the displacement  $\tilde{u}_n$  and independent of the position of the particle. Then the total potential and kinetic energies of the chain can be written in the form

$$\mathbf{V} = \sum_n \frac{1}{2} E \varepsilon \left( \frac{\tilde{u}_{n+1} - \tilde{u}_n}{\varepsilon} \right)^2 + \varepsilon [w(\tilde{u}_n) - \tilde{\sigma} \tilde{u}_n], \quad (2)$$

$$\mathbf{K} = \sum_n \frac{1}{2} \rho \varepsilon \dot{\tilde{u}}_n^2, \quad (3)$$

where  $\varepsilon$  is the reference length,  $E$  is the elastic modulus of the harmonic coupling and  $\rho$  is the mass density per unit spring length. For our choice of the “on-site” potential (1) the general equations of motion

$$\rho \varepsilon \ddot{\tilde{u}}_n - \frac{E}{\varepsilon} (\tilde{u}_{n+1} - 2\tilde{u}_n + \tilde{u}_{n-1}) + \varepsilon [w'(\tilde{u}_n) - \tilde{\sigma}] = 0 \quad (4)$$

can be rewritten in the form

$$\rho \varepsilon \ddot{\tilde{u}}_n - \frac{E}{\varepsilon} (\tilde{u}_{n+1} - 2\tilde{u}_n + \tilde{u}_{n-1}) = \begin{cases} \varepsilon (\tilde{\sigma} - c_1 \tilde{u}_n), & \tilde{u}_n < a/2, \\ \varepsilon [\tilde{\sigma} - c_2 (\tilde{u}_n - a)], & \tilde{u}_n > a/2. \end{cases} \quad (5)$$

Consider now a special class of solutions to Eq. (5) in the form of discrete traveling waves with displacements depending on  $n$  and  $t$  only through  $\tilde{x} = \varepsilon n - \tilde{v}t$ . We assume that

in the moving coordinate system all springs located at  $\tilde{x} > 0$  are in the first energy well (phase 1) and at  $\tilde{x} < 0$  are in the second energy well (phase 2). This ansatz eliminates the possibility of repeated transition between the phases and allows one to focus on an isolated defect. Eq. (5) can then be rewritten in the form

$$\rho\varepsilon\tilde{v}^2 \frac{d^2\tilde{u}}{d\tilde{x}^2} - \frac{E}{\varepsilon} [\tilde{u}(\tilde{x} + \varepsilon) - 2\tilde{u}(\tilde{x}) + \tilde{u}(\tilde{x} - \varepsilon)] + \varepsilon[c_1\tilde{u}(\tilde{x}) - \tilde{\sigma}] - \varepsilon[ac_2 + (c_1 - c_2)\tilde{u}(\tilde{x})]H(-\tilde{x}) = 0, \quad (6)$$

where  $H$  is the Heaviside function. To non-dimensionalize the problem we accept inertial scaling and define

$$x = \frac{\tilde{x}}{\varepsilon}, \quad u = \frac{\tilde{u}}{a}, \quad v = \tilde{v}\sqrt{\frac{\rho}{E}}, \quad \sigma = \frac{\tilde{\sigma}}{ac_1}. \quad (7)$$

Then the main dimensionless parameters of the problem are

$$\Omega_0 = \varepsilon\sqrt{\frac{c_1}{E}}; \quad \Omega_1 = \varepsilon\sqrt{\frac{c_2}{E}}. \quad (8)$$

Note that both parameters  $\Omega_0$  and  $\Omega_1$  depend on the degree of coupling between the bi-stable units: in the continuum case (strong coupling) they are both small, while in the strongly discrete case (loose coupling) they are both large. Therefore, to separate the effects of discreteness from the effects of the asymmetry of the wells we can replace  $\Omega_1$  with another non-dimensional parameter  $\lambda = \sqrt{c_2/c_1}$ . The symmetric case  $\lambda = 1$  has been considered previously (e.g. Kresse and Truskinovsky, 2003) and here we focus on the case when  $\lambda \neq 1$ .

In dimensionless form the linear differential advance–delay equation (6) reads

$$v^2 \frac{d^2u}{dx^2} - [u(x+1) - 2u(x) + u(x-1)] + \Omega_0^2[u(x) - \sigma] - H(-x)[\Omega_1^2 + (\Omega_0^2 - \Omega_1^2)u(x)] = 0, \quad (9)$$

where for consistency we must require

$$u(0) = 1/2, \quad (10)$$

and

$$u(x) < 1/2, x > 0; \quad u(x) > 1/2, x < 0. \quad (11)$$

The last two inequalities oblige the solution on both sides of the defect to stay inside the designated energy wells and play the role of admissibility conditions.

Configurations of the chain at  $x = \pm\infty$  must correspond to the (trivial) static equilibrium with all springs either in one or another well. We assume that at  $x = +\infty$  the crystal remains intact, i.e. all the springs are in phase 1 and  $u = \sigma$ ; at  $x = -\infty$  we assume that  $u = 1 + (\Omega_0^2/\Omega_1^2)\sigma$  meaning that all springs have transformed into phase 2. Therefore

$$u(x) \rightarrow \begin{cases} \sigma, & x \rightarrow \infty, \\ 1 + \frac{\Omega_0^2}{\Omega_1^2}\sigma, & x \rightarrow -\infty. \end{cases} \quad (12)$$

Since one can expect a non-zero radiation of elastic waves at  $x = \pm\infty$ , these limits should be understood in a weak sense as describing only the average values.

### 3. Solution of the discrete problem

In this section, we construct an explicit solution of Eqs. (9)–(12) by adopting some of the analytical tools developed for different but related problems in Slepyan (1981, 2000, 2001a,b,c, 2002), Slepyan and Troyankina (1984) and Marder and Gross (1995).

#### 3.1. Wiener–Hopf method

We begin by introducing the variables

$$U(x) = u(x) + \frac{\Omega_1^2}{\Omega_0^2 - \Omega_1^2}, \quad S = \sigma + \frac{\Omega_1^2}{\Omega_0^2 - \Omega_1^2} \quad (13)$$

allowing one to rewrite Eq. (9) in the simpler form

$$\begin{aligned} v^2 \frac{d^2 U}{dx^2} - [U(x+1) - 2U(x) + U(x-1)] + \Omega_0^2 [U(x) - S] \\ - (\Omega_0^2 - \Omega_1^2) U(x) H(-x) = 0. \end{aligned} \quad (14)$$

Eq. (14) can be solved analytically using the Wiener–Hopf technique. To make the Fourier integrals converge we formally add a factor  $\exp(-\beta|x|)$  to a constant term in Eq. (14) expecting that  $\beta$  is put equal to zero at the end of the calculations. We obtain

$$\begin{aligned} v^2 \frac{d^2 U}{dx^2} - [U(x+1) - 2U(x) + U(x-1)] + \Omega_0^2 U(x) \\ - \Omega_0^2 S e^{-\beta|x|} - (\Omega_0^2 - \Omega_1^2) U(x) H(-x) = 0. \end{aligned} \quad (15)$$

Next we define

$$\hat{U}^\pm(k) = \int_{-\infty}^{+\infty} H(\pm x) U(x) e^{ikx} dx \quad (16)$$

and write the Fourier transform of  $U(x)$  in the form

$$\hat{U}(k) = \hat{U}^-(k) + \hat{U}^+(k). \quad (17)$$

Observe that by construction  $\hat{U}^+$  is free of poles in the upper complex half-plane, while  $\hat{U}^-$  is free of poles in the lower half-plane. In the Fourier space the equation of motion (15) takes the form

$$\hat{U}(k)F(k) + (\Omega_1^2 - \Omega_0^2)\hat{U}^-(k) = \Omega_0^2 S \left( \frac{1}{\beta + ik} + \frac{1}{\beta - ik} \right). \quad (18)$$

By noticing that the last term in Eq. (18) tends to a  $\delta$ -function when  $\beta \rightarrow 0$  we can further rewrite (18) as

$$\hat{U}^+(k)F(k) + \hat{U}^-(k)G(k) = \Omega_0^2 S \left( \frac{1}{0 + ik} + \frac{1}{0 - ik} \right), \quad (19)$$



where

$$\begin{aligned} F(k) &= \Omega_0^2 + 4 \sin^2 \frac{k}{2} - k^2 v^2, \\ G(k) &= \Omega_1^2 + 4 \sin^2 \frac{k}{2} - k^2 v^2. \end{aligned} \quad (20)$$

We can now apply the standard factorization methods to obtain (e.g. Noble, 1958)

$$\begin{aligned} F(k) &= f_-(k)f_+(k), \\ G(k) &= g_-(k)g_+(k), \end{aligned} \quad (21)$$

where the functions  $f_-(k)$  and  $g_-(k)$  are free of poles and zeroes in the lower complex half-plane ( $\text{Im } k < 0$ ), and  $f_+(k)$  and  $g_+(k)$  are free of poles and zeroes in the upper complex half-plane ( $\text{Im } k > 0$ ). Eq. (19) can now be rewritten as

$$\hat{U}^+(k) \frac{f_+(k)}{g_+(k)} + \hat{U}^-(k) \frac{g_-(k)}{f_-(k)} = \frac{\Omega_0^2 S}{g_+(k)f_-(k)} \left( \frac{1}{0+ik} + \frac{1}{0-ik} \right). \quad (22)$$

Since the last term in this equation represents a  $\delta$ -function, we can replace  $g_+(k)$  and  $f_-(k)$  by  $g_+(0) = \Omega_1$  and  $f_-(0) = \Omega_0$  to obtain

$$\hat{U}^+(k) \frac{f_+(k)}{g_+(k)} - \frac{\Omega_0}{\Omega_1} S \frac{1}{0-ik} = \frac{\Omega_0}{\Omega_1} S \frac{1}{0+ik} - \hat{U}^-(k) \frac{g_-(k)}{f_-(k)}. \quad (23)$$

The left-hand side of Eq. (23) is regular in the upper half-plane, while the right side is regular in the lower half-plane. Since the two half-planes overlap at  $k=0$ , each of the two functions can be considered as an analytic continuation of the other and because each function is bounded at infinity they must be equal to the same constant  $C$ . This constant must vanish, to eliminate a delta-type singularity at  $x=0$ . Therefore from Eq. (23) we obtain

$$\hat{U}^+(k) = \frac{\Omega_0}{\Omega_1} \frac{S}{0-ik} \frac{g_+(k)}{f_+(k)}, \quad \hat{U}^-(k) = \frac{\Omega_0}{\Omega_1} \frac{S}{0+ik} \frac{f_-(k)}{g_-(k)}. \quad (24)$$

The next step is to invert the Fourier transforms. We replace  $k$  by  $-k$  and apply Eq. (13) to obtain an implicit representation for the displacement field

$$\begin{aligned} u(x) &= \\ &\begin{cases} \frac{\Omega_0}{\Omega_1} \frac{1}{2\pi i} \left( \sigma + \frac{\Omega_1^2}{\Omega_0^2 - \Omega_1^2} \right) \int_{-\infty}^{+\infty} \frac{1}{k-i0} \frac{g_+(-k)}{f_+(-k)} e^{ikx} dk - \frac{\Omega_1^2}{\Omega_0^2 - \Omega_1^2}, & x > 0, \\ -\frac{\Omega_0}{\Omega_1} \frac{1}{2\pi i} \left( \sigma + \frac{\Omega_1^2}{\Omega_0^2 - \Omega_1^2} \right) \int_{-\infty}^{+\infty} \frac{1}{k+i0} \frac{f_-(-k)}{g_-(-k)} e^{ikx} dk - \frac{\Omega_1^2}{\Omega_0^2 - \Omega_1^2}, & x < 0. \end{cases} \end{aligned} \quad (25)$$

In order to compute the integral at  $x > 0$  we need to close the contour of integration in the upper half-plane including the poles at  $k=i0$  and at zeros of  $f_+(-k)=0$ . Similarly the displacement field at  $x < 0$  is determined by the roots of  $g_-(-k)=0$  in the lower half-plane and the pole at  $k=-i0$ .

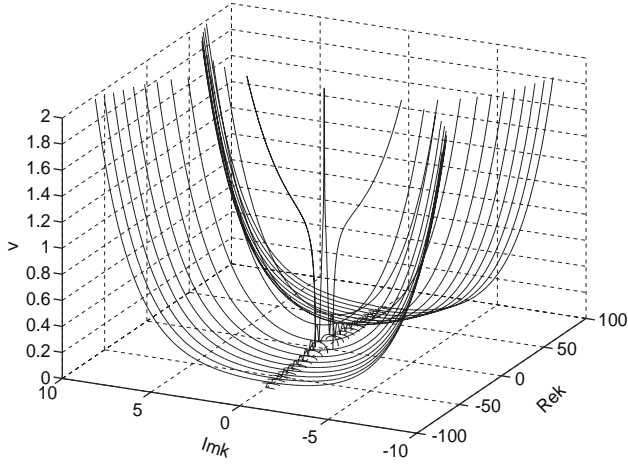


Fig. 3. Complex dispersion spectrum ahead of the kink,  $F(k) = 0$ , for  $\Omega_0 = 0.5$ .

### 3.2. Analysis of the dispersion relation

In order to write solution (25) explicitly we need to identify the relevant zeroes of the functions  $f_{\pm}(k)$  and  $g_{\pm}(k)$ . We begin with a review of the broader set of roots of the dispersion relations

$$F(k) = 0, \quad G(k) = 0. \quad (26)$$

These relations are saying that the phase speed of the emitted waves must be equal to the speed of the kink ahead and behind the front, respectively. From Fig. 3 one can see that for the given  $v$  there are always a finite number of real roots of the dispersion relation, representing non-decaying propagating waves which carry energy away from the front. In addition, there are exactly two symmetric purely imaginary roots, determining the non-oscillatory structure of the displacement field near the core of the defect. Finally, there are infinite number of symmetric complex roots which are located in all four quadrants of the complex plane and determine the oscillatory structure in the core region.

We begin with the analysis of the real roots. Graphically they can be obtained as the intersection of the curves  $\Omega_{F,G} = \sqrt{\Omega_{0,1}^2 + 4 \sin^2 k/2}$  with the straight line  $\Omega = kv$  (see Fig. 4a). Depending on the value of  $v$  equation  $F(k) = 0$  can have one, three, etc. simple solutions on the real axis: the corresponding roots  $\pm r_v$  ( $v = 1, 2, \dots, 2l + 1$ ) form an increasing sequence; similar roots of the equation  $G(k) = 0$  will be denoted by  $\pm p_v$  ( $v = 1, 2, \dots, 2m + 1$ ). The relevant real roots are selected by the radiation condition stating that ahead of the moving kink the group velocity of the radiated waves  $v_g = d\Omega/dk$  must be larger than the phase velocity  $v = \Omega/k$ . Accordingly, behind the kink, the group velocity must be smaller than the phase velocity. The radiation condition reflects the fact that if the group velocity is smaller then the phase velocity

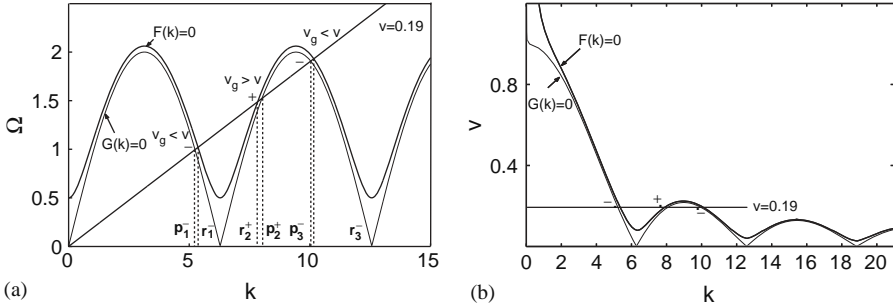


Fig. 4. The real roots of the dispersion relations  $F(k)=0$  and  $G(k)=0$  for  $\Omega_0=0.5$ ,  $\Omega_1=0.01$  and  $v=0.19$ .

( $v_g < v$ ), introduction of a small viscosity shifts the real roots selected by the radiation condition ahead and behind the front, respectively, we introduce the superscripts  $+$  and  $-$  and obtain:  $r_v^+$  where  $v = 2, 4, \dots, 2l$  and  $r_v^-$  where  $v = 1, 3, \dots, 2l + 1$  (see Fig. 4). The same procedure, applies to the real roots  $p_v^\pm$  of  $G(k) = 0$ , generates the sequences  $p_1^-, p_3^-, \dots, p_{2m+1}^-$  and  $p_2^+, p_4^+, \dots, p_{2m}^+$  (see Fig. 4).

$$v_g - v = \frac{1}{2vk} [F, G]'(k). \quad (27)$$

Now we can write more precisely the expressions for  $f_\pm(k)$  and  $g_\pm(k)$  in Eq. (21). Due to the symmetry of the roots (26) we can write (e.g. Noble, 1958)

$$F(k) = \Omega_0^2 \prod_{v=1,3,\dots}^{2l+1} \left[ 1 + \left( \frac{0+ik}{r_v^-} \right)^2 \right] \prod_{v=2,4,\dots}^{2l} \left[ 1 + \left( \frac{0-ik}{r_v^+} \right)^2 \right] \Phi(k),$$

$$G(k) = \Omega_1^2 \prod_{v=1,3,\dots}^{2m+1} \left[ 1 + \left( \frac{0+ik}{p_v^-} \right)^2 \right] \prod_{v=2,4,\dots}^{2m} \left[ 1 + \left( \frac{0-ik}{p_v^+} \right)^2 \right] \Gamma(k), \quad (28)$$

where only real roots of the dispersion relation have been explicitly identified. The positive (and even) functions  $\Phi(k)$  and  $\Gamma(k)$  both have an infinite number of complex roots which can be organized in symmetric sets of quadruples. Therefore we can write

$$\Phi(k) = \Phi_+(ik)\Phi_-(ik), \quad \Gamma(k) = \Gamma_+(ik)\Gamma_-(ik), \quad (29)$$

where  $\Phi_\pm(ik)$  (and  $\Gamma_\pm(ik)$ ) represent complex conjugate functions. Note also that both  $\Phi_+$  and  $\Gamma_+$  have neither zeros nor poles in the upper complex half-plane (including the real axis). Similarly neither  $\Phi_-$  nor  $\Gamma_-$  have poles or zeros in the lower half-plane.

Denote by  $\pm a_v \pm ib_v$  the complex roots of  $F(k)=0$  and by  $\pm c_v \pm id_v$  the complex roots of  $G(k)=0$ . Then due to the symmetry of the roots with respect to the real axis,

we can represent the functions  $\Phi_{\pm}$  and  $\Gamma_{\pm}$  as

$$\begin{aligned}\Phi_+(ik) &= \prod_1^{\infty} \left(1 - \frac{k^2 + 2ib_v k}{a_v^2 + b_v^2}\right); \quad \Phi_-(ik) = \prod_{v=1}^{\infty} \left(1 - \frac{k^2 - 2ib_v k}{a_v^2 + b_v^2}\right), \\ \Gamma_+(ik) &= \prod_1^{\infty} \left(1 - \frac{k^2 + 2id_v k}{c_v^2 + d_v^2}\right); \quad \Gamma_-(ik) = \prod_{v=1}^{\infty} \left(1 - \frac{k^2 - 2id_v k}{c_v^2 + d_v^2}\right).\end{aligned}\quad (30)$$

This allows us to finalize the factorization (21) in the form

$$\begin{aligned}f_-(-k) &= \Omega_0 \left(1 + \frac{k}{i\eta_r}\right) \prod_{v=1,3,\dots}^{2l+1} \left(1 - \frac{k^2}{r_v^{-2}}\right) \prod_{v=1}^{\infty} \left(1 - \frac{k^2 + 2ib_v k}{a_v^2 + b_v^2}\right), \\ g_+(-k) &= \Omega_1 \left(1 - \frac{k}{i\eta_p}\right) \prod_{v=2,4,\dots}^{2m} \left(1 - \frac{k^2}{p_v^{+2}}\right) \prod_{v=1}^{\infty} \left(1 - \frac{k^2 - 2id_v k}{c_v^2 + d_v^2}\right), \\ f_+(-k) &= \Omega_0 \left(1 - \frac{k}{i\eta_r}\right) \prod_{v=2,4,\dots}^{2l} \left(1 - \frac{k^2}{r_v^{+2}}\right) \prod_{v=1}^{\infty} \left(1 - \frac{k^2 - 2ib_v k}{a_v^2 + b_v^2}\right), \\ g_-(-k) &= \Omega_1 \left(1 + \frac{k}{i\eta_p}\right) \prod_{v=1,3,\dots}^{2m+1} \left(1 - \frac{k^2}{p_v^{-2}}\right) \prod_{v=1}^{\infty} \left(1 - \frac{k^2 + 2id_v k}{c_v^2 + d_v^2}\right).\end{aligned}\quad (31)$$

To write the solution in explicit form we now need to replace the first integral in Eq. (25) by the contour integral which follows the real axis and passes below singular points  $k = 0$  and  $k = r_v^+$  and above singular points  $k = r_v^-$ . Similarly, for  $x < 0$  the second integral in Eq. (25) can be replaced by the integral along the closed contour along the real axis, above  $k = 0$  and  $p_v^-$  and below  $k = p_v^+$ . Then by using the method of residues we obtain

$$u(x) = \begin{cases} \sigma + \frac{\Omega_0}{\Omega_1} \left(\sigma + \frac{\Omega_1^2}{\Omega_0^2 - \Omega_1^2}\right) \sum_{k \in \mathcal{F}_+} A^+(k) e^{ikx}, & x > 0, \\ 1 + \frac{\Omega_0^2}{\Omega_1^2} \sigma + \frac{\Omega_0}{\Omega_1} \left(\sigma + \frac{\Omega_1^2}{\Omega_0^2 - \Omega_1^2}\right) \sum_{k \in \mathcal{G}_-} A^-(k) e^{ikx}, & x < 0, \end{cases}\quad (32)$$

where

$$\begin{aligned}\sum_{k \in \mathcal{F}_+} A^+(k) e^{ikx} &= \sum_{\substack{v=2,4,\dots \\ k=\pm r_v^+}}^{2l} \frac{g_+(-k)}{k f'_+(-k)} e^{ikx} + \frac{g_+(-k)}{k f'_+(-k)} e^{ikx} \Big|_{k=i\eta_r} \\ &+ \sum_{\substack{v=1,2,\dots \\ k=\pm a_v + ib_v}}^{\infty} \frac{g_+(-k)}{k f'_+(-k)} e^{ikx},\end{aligned}$$

$$\begin{aligned}
\sum_{k \in \mathcal{G}_-} A^-(k) e^{ikx} &= \sum_{\substack{v=1,3,\dots \\ k=\pm p_v^-}}^{2m+1} \frac{f_-(-k)}{kg'_-(-k)} e^{ikx} + \frac{f_-(-k)}{kg'_-(-k)} e^{ikx} \Big|_{k=-in_p} \\
&+ \sum_{\substack{v=1,2,\dots \\ k=\pm c_v - id_v}}^{\infty} \frac{f_-(-k)}{kg'_-(-k)} e^{ikx}.
\end{aligned} \tag{33}$$

We remark that the residue at  $k = 0$  is responsible for the homogeneous part of the displacement field in Eq. (32). To complete the solution we need to specify the force–velocity relation  $\sigma(v)$ .

### 3.3. Force–velocity relation

To find the function  $\sigma(v)$  we must use the matching condition  $u(0) = \frac{1}{2}$ . Since the function  $U(x)$  is continuous, we obtain

$$U(0) = \lim_{x \rightarrow 0} U(x) = \lim_{k \rightarrow \infty} k \sqrt{\hat{U}^+(ik) \hat{U}^-( -ik)}, \tag{34}$$

where the functions  $\hat{U}^\pm(k)$  are defined by Eq. (16). Then, from Eqs. (34) and (24) we can write

$$\lim_{x \rightarrow 0} U(x) = \frac{\Omega_0}{\Omega_1} S \lim_{k \rightarrow \infty} \sqrt{\frac{g_+(ik) f_-(-ik)}{f_+(ik) g_-(-ik)}}, \tag{35}$$

where according to Eq. (31)

$$\begin{aligned}
\frac{g_+(ik) f_-(-ik)}{f_+(ik) g_-(-ik)} &= \prod_{v=2,4,\dots}^{2m} \frac{(p_v^+)^2 + k^2}{(p_v^+)^2} \prod_{v=1,3,\dots}^{2l+1} \frac{(r_v^-)^2 + k^2}{(r_v^-)^2} \\
&\times \prod_{v=2,4,\dots}^{2l} \frac{(r_v^+)^2}{(r_v^+)^2 + k^2} \prod_{v=2,4,\dots}^{2m+1} \frac{(p_v^-)^2}{(p_v^-)^2 + k^2} \times \frac{\Gamma_+(-k) \Phi_-(k)}{\Phi(-k) \Gamma_-(k)}.
\end{aligned}$$

Analysis of Eq. (30) shows that

$$\begin{aligned}
\frac{\Phi_+(-k)}{\Phi_-(k)} &\rightarrow 1, k \rightarrow \infty; \Phi_\pm \rightarrow 1, k \rightarrow 0, \\
\frac{\Gamma_+(-k)}{\Gamma_-(k)} &\rightarrow 1, k \rightarrow \infty; \Gamma_\pm \rightarrow 1, k \rightarrow 0.
\end{aligned} \tag{36}$$

Therefore, Eq. (35) can be rewritten as

$$\begin{aligned}
U(0) &= \lim_{x \rightarrow 0} U(x) = \frac{\Omega_0}{\Omega_1} S \lim_{k \rightarrow \infty} \sqrt{\prod \frac{(r_v^+)^2 (p_v^-)^2}{(p_v^+)^2 (r_v^-)^2}} \\
&\times \sqrt{\prod_{v=2,4,\dots}^{2m} \left(1 + \frac{(p_v^+)^2}{k^2}\right) \prod_{v=1,3,\dots}^{2l+1} \left(1 + \frac{(r_v^-)^2}{k^2}\right) \prod_{v=2,4,\dots}^{2l} \left(1 + \frac{(r_v^+)^2}{k^2}\right)^{-1} \prod_{v=2,4,\dots}^{2m+1} \left(1 + \frac{(p_v^-)^2}{k^2}\right)^{-1}} \\
&= \frac{\Omega_0}{\Omega_1} S \prod \frac{r_v^+ p_v^-}{p_v^+ r_v^-}. \tag{37}
\end{aligned}$$

By combining Eq. (37) with (13) we obtain the desired force–velocity relation

$$\sigma = \left( \frac{1}{2} + \frac{\Omega_1^2}{\Omega_0^2 - \Omega_1^2} \right) \frac{\Omega_1}{\Omega_0} \prod \frac{p_v^+ r_v^-}{p_v^- r_v^+} - \frac{\Omega_1^2}{\Omega_0^2 - \Omega_1^2}. \tag{38}$$

Note that since the roots  $r_v^\pm$  and  $p_v^\pm$  are real and positive, the force–velocity relation is determined exclusively by the radiative modes. We begin the analysis of Eq. (38) by first identifying the limits of the function  $\sigma(v)$  at  $v \rightarrow +\infty$  and  $v \rightarrow 0$ :

1. As  $v \rightarrow \infty$  we are left with only two roots  $k = r_1^-$  and  $k = p_1^-$  and can write

$$\lim_{v \rightarrow \infty} \sigma = \lim_{v \rightarrow \infty} \left( \frac{1}{2} + \frac{\Omega_1^2}{\Omega_0^2 - \Omega_1^2} \right) \frac{\Omega_1}{\Omega_0} \frac{r_1^-}{p_1^-} - \frac{\Omega_1^2}{\Omega_0^2 - \Omega_1^2}. \tag{39}$$

By using expressions for  $k = r_1^-$  and  $k = p_1^-$

$$r_1^- = \frac{1}{v} \sqrt{\Omega_0^2 - 4 \sin^2 \frac{r_1^-}{2}}, \quad p_1^- = \frac{1}{v} \sqrt{\Omega_1^2 - 4 \sin^2 \frac{p_1^-}{2}}, \tag{40}$$

we obtain

$$\frac{r_1^-}{p_1^-} = \xrightarrow{v \rightarrow \infty} \frac{\Omega_0}{\Omega_1}. \tag{41}$$

This gives

$$\lim_{v \rightarrow \infty} \sigma = \frac{1}{2}. \tag{42}$$

To interpret the right-hand side of Eq. (42) we notice that the boundary conditions (12) are compatible with the admissibility conditions if and only if  $-\Omega_1^2/2\Omega_0^2 < \sigma < \frac{1}{2}$  where the limiting values represent the ultimate (spinodal) strength of the snap-springs in “tension” and “compression”, respectively. We conclude that the velocity of the kink increases indefinitely when the applied force approaches the maximum value supported by each of the phases.

2. Finding the limit of the force–velocity relation at  $v \rightarrow 0$  is not that straightforward. The difficulty in treating this case arises from the fact that the number of the relevant roots increases rapidly as  $v$  tends to zero. Note, however, that for small velocities the line  $\Omega = kv$  is almost horizontal and therefore we can write the approximate expressions

for the real roots of the dispersion relations (26) in the form

$$r_i^\pm = 2 \left[ (n_0 + i)\pi \pm \sin^{-1} \sqrt{v^2(n_0 + i)^2\pi^2 - \frac{\Omega_0^2}{4}} \right],$$

$$p_j^\pm = 2 \left[ (m_0 + j)\pi \pm \sin^{-1} \sqrt{v^2(m_0 + j)^2\pi^2 - \frac{\Omega_1^2}{4}} \right]. \quad (43)$$

Here  $i$  is an integer which varies between  $n_0$  to  $n_f$ ; to find  $n_0$  and  $n_f$  we need to compute the integer parts for the solution of the system  $2\pi n_0 v = \Omega_0$ ,  $2\pi(n_0 + n_f)v = \sqrt{\Omega_0^2 + 4}$ . Similarly,  $j$  is an integer varying between  $m_0$  and  $m_f$  which both can be obtained from the system  $2\pi m_0 v = \Omega_1$ ,  $2\pi(m_0 + m_f)v = \sqrt{\Omega_1^2 + 4}$ . We must also remember that there are always two extra waves behind the kink. Introduce  $P(v) = \prod \frac{p_j^+}{p_j^-} \prod \frac{r_i^-}{r_i^+}$ . By using the above approximations for all the relevant roots, we obtain

$$P(v) \approx \prod_{j=1}^{m_f-1} \frac{(m_0 + j)\pi + \sin^{-1} \sqrt{v^2(m_0 + j)^2\pi^2 - \frac{\Omega_1^2}{4}}}{(m_0 + j)\pi - \sin^{-1} \sqrt{v^2(m_0 + j)^2\pi^2 - \frac{\Omega_1^2}{4}}}$$

$$\times \prod_{i=1}^{n_f-1} \frac{(n_0 + i)\pi - \sin^{-1} \sqrt{v^2(n_0 + i)^2\pi^2 - \frac{\Omega_0^2}{4}}}{(n_0 + i)\pi + \sin^{-1} \sqrt{v^2(n_0 + i)^2\pi^2 - \frac{\Omega_0^2}{4}}}$$

$$\times \frac{(n_0 + n_f)\pi - \sin^{-1} \sqrt{v^2(n_0 + n_f)^2\pi^2 - \frac{\Omega_0^2}{4}}}{(m_0 + m_f)\pi - \sin^{-1} \sqrt{v^2(m_0 + m_f)^2\pi^2 - \frac{\Omega_1^2}{4}}}. \quad (44)$$

Therefore

$$\ln P \approx \frac{1}{2} \ln \frac{\Omega_0^2 + 4}{\Omega_1^2 + 4} + \sum_{j=1}^{m_f-1} \frac{2}{(m_0 + j)\pi} \sin^{-1} \sqrt{v^2(m_0 + j)^2\pi^2 - \frac{\Omega_1^2}{4}}$$

$$- \sum_{i=1}^{n_f-1} \frac{2}{(n_0 + i)\pi} \sin^{-1} \sqrt{v^2(n_0 + i)^2\pi^2 - \frac{\Omega_0^2}{4}}. \quad (45)$$

In the limit  $v \rightarrow 0$  we can switch from summation to integration to obtain  $\ln P \approx \ln \frac{\Omega_0 + \sqrt{\Omega_0^2 + 4}}{\Omega_1 + \sqrt{\Omega_1^2 + 4}}$ . Finally from Eq. (38) we compute the desired limit

$$\lim_{v \rightarrow 0} \sigma = \left( \frac{1}{2} + \frac{\Omega_1^2}{\Omega_0^2 - \Omega_1^2} \right) \frac{\Omega_1}{\Omega_0} \frac{\Omega_0 + \sqrt{\Omega_0^2 + 4}}{\Omega_1 + \sqrt{\Omega_1^2 + 4}} - \frac{\Omega_1^2}{\Omega_0^2 - \Omega_1^2}. \quad (46)$$

As we show in the Appendix the right-hand side of Eq. (46) coincides with the expression for the static Peierls force  $\sigma_p^+$ . This confirms that the dynamic regimes describing steadily propagating kinks can be viewed as “bifurcating” from the static solutions corresponding to pinned kinks. The fine structure of the resulting “bifurcation” is quite

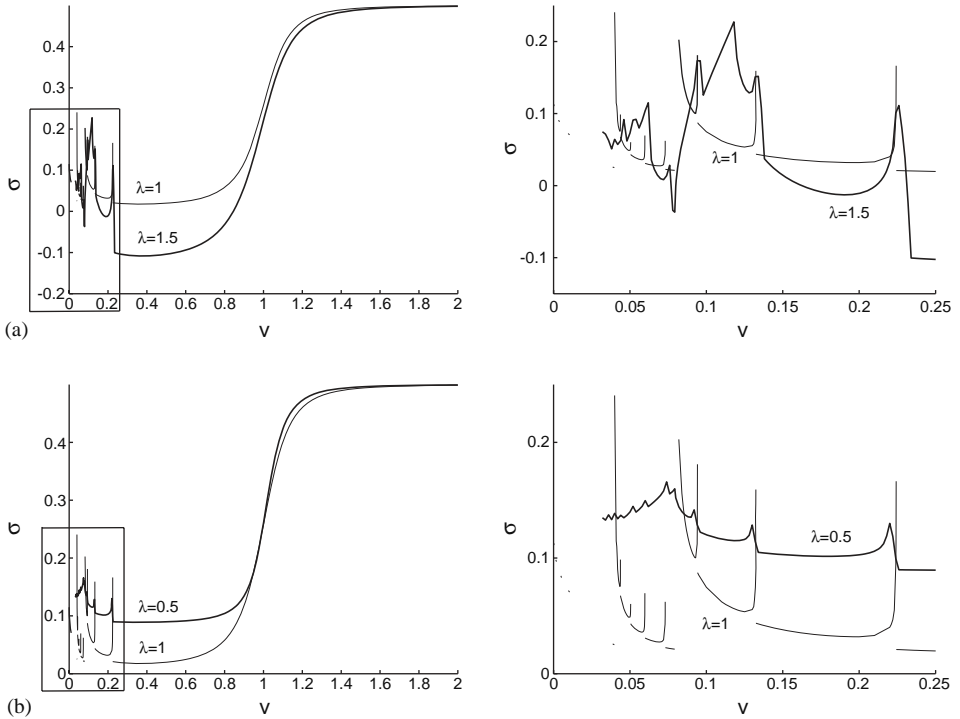


Fig. 5. Comparison of the force–velocity relations for the cases: (a)  $\Omega_1 = 0.5$  ( $\lambda = 1.0$ ) and  $\Omega_1 = 0.75$  ( $\lambda = 1.5$ ), (b)  $\Omega_1 = 0.5$  ( $\lambda = 1.0$ ) and  $\Omega_1 = 0.25$  ( $\lambda = 0.5$ ). The figures on the right represent the blow up of the selected areas on the left. In all graphs  $\Omega_0 = 0.5$ .

complex because of the accumulation of the infinite number of (mostly unstable) dynamic branches; in view of the presence of the kinks propagating at sub-Peierls stresses it can be characterized as sub-critical.

To illustrate the global force–velocity relation one needs to compute numerically the exact location of the relevant roots of the dispersion relations and substitute the corresponding values of  $k$  into Eq. (38). Several representative graphs for  $\sigma(v)$  are shown in Fig. 5. We observe that in the over-symmetric case  $\Omega_1 = \Omega_0$  ( $\lambda = 1$ , dislocation) the system experiences infinite resonances at critical velocities where phase and group velocities coincide ( $v_g = v$ ) and as a result either  $r_v^+ = r_v^-$  or  $p_v^+ = p_v^-$  (see Atkinson and Cabrera, 1965; Peyrard and Kruskal, 1984; Kresse and Truskinovsky, 2003; for the detailed discussion of this case). Although the resonances disappear when  $\Omega_1 \neq \Omega_0$ , the function  $\sigma(v)$  continues to experience visible “disturbances” near the resonant velocities  $v_*^f$  and  $v_*^g$  in front and behind the kink, respectively. These special velocities correspond, according to Eq. (27), to the real wavenumbers  $k$  which satisfy the equations  $F(k, v) = 0, F'_k(k, v) = 0$  in front and equations  $G(k, v) = 0, G'_k(k, v) = 0$  behind the kink.

In Fig. 6a we present the typical displacement fields for the velocity interval  $v > \max\{v_{*1}^f, v_{*1}^g\}$ , where  $v_{*1}^f$  and  $v_{*1}^g$  are the largest critical velocities. In this



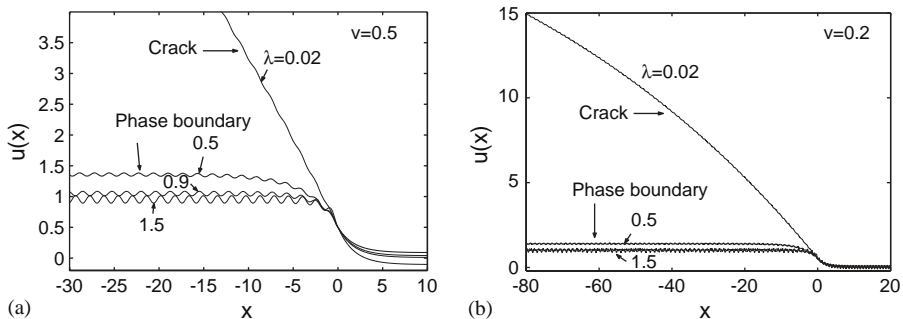


Fig. 6. The displacement profile corresponding to the moving kink at different values of the asymmetry parameter  $\lambda$ . The steady-state velocities are taken from two intervals: where radiation exists only behind the kink,  $v=0.5$  (a), and where radiation is present both ahead and behind the kink  $v=0.2$  (b). In both figures  $\Omega_0 = 0.5$ .

velocity interval we have only two relevant real roots of the dispersion relations:  $r_1^-$  and  $p_1^-$ . Since at  $x > 0$  we take into account only roots with even subscripts, there are no radiative modes ahead of the defect and the only radiative mode (with the wave number  $k = p_1^-$ ) appears behind the defect. For comparison we also show a representative profile from another velocity interval,  $\max\{v_{*2}^f, v_{*2}^g\} < v < \min\{v_{*1}^f, v_{*1}^g\}$ , where  $v_{*2}^f$  and  $v_{*2}^g$  are next to largest critical velocities. In this interval the dispersion equations (26) have six relevant real roots:  $r_1^-, r_2^+, r_3^-$  and  $p_1^-, p_2^+, p_3^-$ . By eliminating the modes prohibited by the radiation conditions we obtain one propagating mode ahead the front (with the wave number  $r_2^+$ ) and two propagating modes behind the defect (with the wave numbers  $p_1^-, p_3^-$ ) (see Fig. 6). Note that in both cases shown in Fig. 6 the radiative damping manifests itself through the presence in the displacement profile of the non-decaying oscillatory tails. The structure of the profile changes considerably when the asymmetry parameter varies from  $\lambda = 1$ , corresponding to the case of a dislocation, to near  $\lambda = 0$ , corresponding to the case of a crack. This reflects the fact that in the case of dislocations we prescribe displacement discontinuity while in the case of fracture we implicitly apply zero tractions on the surfaces of the crack (see Fig. 6).

An interesting feature of the highly asymmetrical case, when the modulus of the second phase is very small, is the apparent morphological instability of the displacement profile. For instance in the case  $\Omega_0 = 0.5$ ,  $\Omega_1 = 0.01$  our Fig. 7 demonstrates fast growth of the amplitude of the oscillations behind the front of the defect around a critical velocity  $v \approx 0.8$ . This phenomenon may be related to the branching instability of the fast moving cracks observed experimentally (e.g. Fineberg and Marder, 1999).

### 3.4. Admissibility conditions

To complete the construction of the solution we need to check that Eqs. (32)–(33) and (38) satisfy the admissibility conditions (11). To see the origin of possible non-admissibility (noticed also in the related context by Earmme and Weiner, 1977; Marder and Gross, 1995), we need to examine the fine structure of the

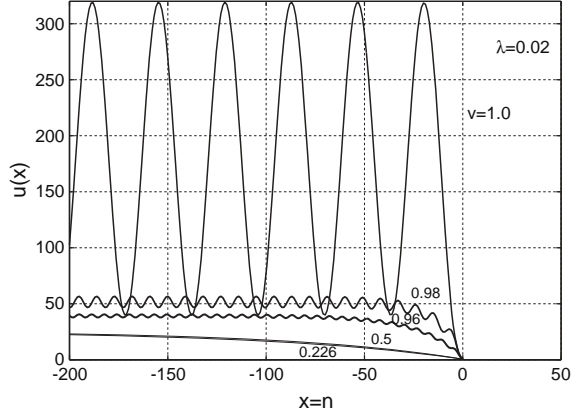


Fig. 7. Development of large oscillations in the displacement profile near critical velocity at  $\Omega_1 = 0.01$ ,  $\Omega_0 = 0.5$  ( $\lambda = 0.02$ ) and  $v > v_{*1}^f = 0.2243$ .

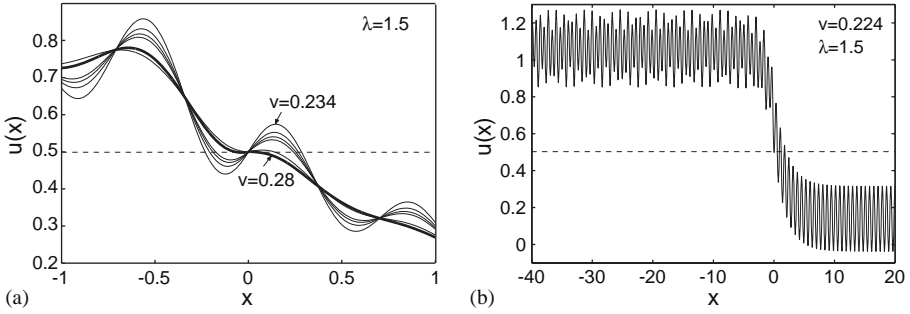


Fig. 8. The displacement field near the core region of the defect for  $\lambda = 1.5$  ( $\Omega_0 = 0.5$  and  $\Omega_1 = 0.75$ ): (a) in the first velocity interval  $v > \max\{v_{*1}^f, v_{*1}^g\}$ —solution is admissible for  $v > 0.27$ , (b) for  $v = 0.224$  from the second velocity interval  $\max\{v_{*2}^f, v_{*2}^g\} < v < \min\{v_{*1}^f, v_{*1}^g\}$ —solution is not admissible.

displacement field near the core region of the moving defect. Consider for instance the case when  $\Omega_0 = 0.5$ ,  $\Omega_1 = 0.75$  and  $\lambda = 1.5$ . The first few critical velocities are then equal to  $v_{*1}^f = 0.22427$ ,  $v_{*1}^g = 0.23282$ ,  $v_{*2}^f = 0.13239$ ,  $v_{*2}^g = 0.13727$ . Representative solutions from the velocity interval  $v > \max\{v_{*1}^f, v_{*1}^g\}$ , are presented in Fig. 8a. One can see that in addition to a propagating wave behind the front the typical displacement field contains exponentially damped oscillatory contributions which may force solution to change “phase” before the point  $x = 0$  making it inadmissible. Indeed numerical experiments show that the admissibility conditions in this velocity interval are satisfied only for  $v > 0.27$  (see Fig. 8). In the case of equal moduli  $\Omega_0 = \Omega_1 = 0.5$  ( $\lambda = 1$ ), the admissibility interval is broader  $v > 0.26$  and in general the lower is the elastic modulus of the second phase, the wider is the spectrum of admissible velocities. In the second velocity interval  $\max\{v_{*2}^f, v_{*2}^g\} < v < \min\{v_{*1}^f, v_{*1}^g\}$ , our computations indicate that for  $\lambda = 1.5$

no solution is admissible at all (see Fig. 8). Other numerical experiments produced the following results. We found that for  $\Omega_0 = \Omega_1 = 0.5$  the solution is admissible only at  $v > 0.26$ ; for  $\Omega_0 = 0.5, \Omega_1 = 0.45$ —at  $v > 0.25$  and around  $v = 0.2$ ; for  $\Omega_0 = 0.5, \Omega_1 = 0.25$  the admissibility domain includes the intervals  $v > 0.24$  and  $0.145 < v < 0.215$ . In the case of a very small modulus of the second phase  $\Omega_1 = 0.01$  the admissibility domain is broader and includes the intervals  $v > 0.23$  and  $0.136 < v < 0.217$  at least. In general, the influence of the resonant velocities remains essential for admissibility even far away from the fully resonant case  $\lambda = 1$ .

#### 4. Friction law

As we have seen in the previous sections, the motion of a kink through the lattice is accompanied by generation of lattice scale radiation. The resulting energy transfer from long to short waves reveals itself at the macro-level as dissipation. To compute the dissipative potential  $\mathbf{R}(v)$  we observe that the energy densities associated with homogeneous contributions to the displacement fields at  $\pm\infty$  are different:  $-\frac{1}{2}\Omega_0^2\sigma^2$  at  $x = +\infty$  and  $\Omega_0^2\sigma - (\Omega_0^4/2\Omega_1^2)\sigma^2 + \frac{1}{8}(\Omega_0^2 - \Omega_1^2)$  at  $x = -\infty$ . Then, since the macroscopic motion at  $x = \pm\infty$  is absent, the energy is released at the rate equal to the difference between the limiting energy densities multiplied by the velocity of the defect

$$\mathbf{R}(v) = \left[ \Omega_0^2\sigma + \frac{\Omega_0^2}{2\Omega_1^2}\sigma^2(\Omega_0^2 - \Omega_1^2) - \frac{1}{8}(\Omega_0^2 - \Omega_1^2) \right] v. \quad (47)$$

The dissipative function  $\mathbf{R}(v)$  can be expressed as a product of the configurational force  $G(v)$  and the velocity of the defect  $v$

$$\mathbf{R}(v) = G(v)v, \quad (48)$$

which leads to the following expression for the configurational force  $G$ :

$$G(v) = \Omega_0^2\sigma + \frac{\Omega_0^2}{2\Omega_1^2}\sigma^2(\Omega_0^2 - \Omega_1^2) - \frac{1}{8}(\Omega_0^2 - \Omega_1^2). \quad (49)$$

As we see, except for the case when  $\Omega_0 = \Omega_1$  ( $\lambda = 1$ ), the relation between  $G$  and  $\sigma$  is quadratic. This result has a simple geometrical interpretation. Consider a dimensional force–strain relation for a single bi-stable snap-spring shown in Fig. 9; a straightforward computation shows that  $G(v) = \varepsilon(S_2 - S_1)/(a^2E)$ , where  $S_1$  and  $S_2$  are the marked areas. It is clear that similar area-rule remains valid in the case of a general double-well potential. By substituting Eq. (38) into (49) we obtain the final relation for the configurational force in terms of the wave numbers of the radiated waves

$$G(v) = \frac{1}{2}(\Omega_0^2 - \Omega_1^2) \left( \frac{1}{2} + \frac{\Omega_1^2}{\Omega_0^2 - \Omega_1^2} \right)^2 \left[ \prod \left( \frac{p_i^+ r_i^-}{p_i^- r_i^+} \right)^2 - 1 \right]. \quad (50)$$

The resulting structure of the friction law is illustrated in Fig. 10. The kinetic curves corresponding to different values of parameter  $\lambda$  from dislocations to cracks are consistent: complex, fully discrete behavior at small velocities and more “continuum like” behavior at near sonic and supersonic velocities. One can again see that at critical velocities the drag resistance exhibits quasi-resonant behavior; these small-velocity regimes,

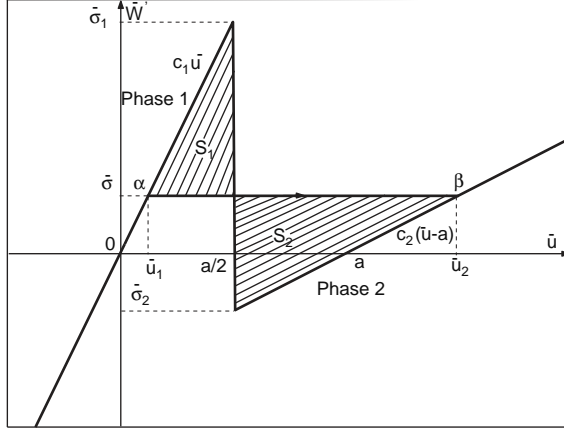


Fig. 9. Geometrical interpretation of the configurational force  $G$ . The transition is from  $\alpha$  to  $\beta$ .

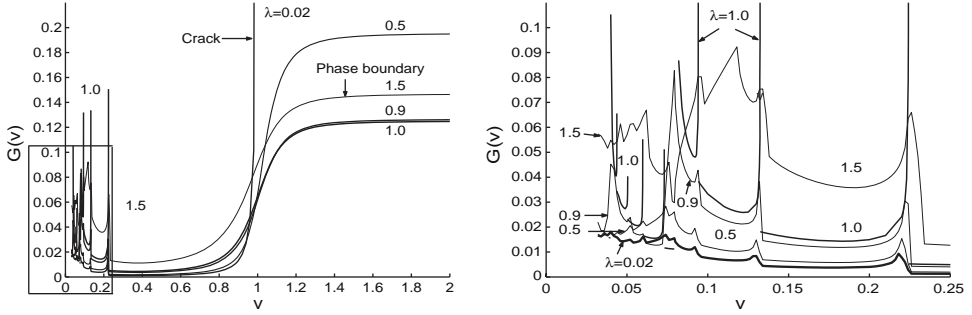


Fig. 10. The friction law for different  $\lambda$  and  $\Omega_0 = 0.5$ . The graph on the right is a blow up of the box on the left.

however, should be mostly disregarded since the corresponding travelling waves are not admissible. With the non-admissible solutions excluded, the overall picture of radiative kinetics can be characterized as dry friction with a characteristic peak in resistance followed by a plateau which eventually gives rise to a singular behavior around sonic velocity. This picture is consistent with observations.

## 5. Conclusions

In this paper, we used the Wiener–Hopf technique to construct a family of closed-form solutions in the fully inertial discrete model describing a steady-state propagation of a generic lattice defect. Our solutions clearly show that in the medium with structure the propagation of the defect can be viewed as an autocatalytic development of a cascade of internal instabilities. This process generates short wave lattice oscillations

which carry energy away from the propagating front and produce radiative damping. The advantage of our formulation is the possibility to trace all the details of the complex oscillatory motion generated by the bond breaking process. Since the only input information concerns with the elasticities of the constitutive elements, the present model qualifies as of “first principle” type. It can be viewed as the generalization of the classical FK model for a moving dislocations which has been known to have a major defect: an infinite sequence of (resonant) velocities where the drag force generated by the lattice is infinite. The traditional way of dealing with these singularities has been either to raise the dimensionality of the problem or to introduce explicit dissipation. Instead in this paper we showed that the singularities can be removed already in the one-dimensional (1D) Hamiltonian framework if we lower the symmetry of the problem. The over-symmetric solution for dislocation appears then as a special case which allows for relatively easy analysis at a price of spurious effects.

We complemented most of the previous work, focused entirely on the kinetic relations, by the study the structure of the displacement field in different velocity intervals, including the regions near the resonances, determining the interval of admissibility of the travelling wave solutions. The systematic investigation of the boundaries of the admissibility regions showed finite gaps in the low velocity domain between the “lattice trapped” states and the domain of fast inertial motions. Contrary to the symmetric case of dislocations where none of the slow solutions in the gap is admissible, in the asymmetric case there exist isolated lagoons of admissibility.

Since, in general, exact solutions of the whole one parametric family of nonlinear discrete problems are rare, our explicit travelling waves with oscillatory structure can be used as a benchmark for numerical simulations, moreover, the access to analytical results also clarifies the structure of the numerically inaccessible “static-dynamic” depinning bifurcation. Overall, the qualitative similarity of the computed friction laws with experimental data suggests that the main features of the model can survive the extension from the present 1D bi-parabolic setting to the case of more general nonlinearities.

In conclusion we mention several limitations of the present model. Note that in our setting the limiting elastic velocity is absent which is a manifestation of the fact that we are dealing with a semi-linear instead of a quasi-linear problem. The study of the corresponding quasi-linear problem which generates in the continuum limit the nonlinear wave equation and in statics reduces to the FK model has been recently initiated by Truskinovsky and Vainchtein (2003, 2004). Another limitation is the 1D character of the present model which at least partially can be overcome by introducing explicit dissipation mimicking the energy escape into the mechanical degrees of freedom not explicitly described by the model. Finally, the main open issue is the stability of the obtained class of solutions. While the non-convexity of the dissipative function at small velocities and the related computations of Marder and Gross (1995) hint towards instability of at least some branches of the kinetic relation, the detailed mathematical analysis, proving nonlinear stability of our travelling waves remains to be done. In the areas where traveling waves are either non-admissible or unstable, the question arises as of the actual nature of dynamic solutions at the corresponding values of the average velocity. Filling these gaps would require the use of a more general non steady ansatz.

## Acknowledgements

This work was supported by the NSF grants DMS-9803572 and DMS-0102841.

## Appendix.

Here we briefly outline solutions of Eqs. (9)–(12) describing lattice trapped defects. In statics the finite-difference equation (9) takes the form

$$u_{n+1} - 2u_n + u_{n-1} + \Omega_0^2 \sigma = \begin{cases} \Omega_0^2 u_n, & n \geq 0, \\ \Omega_1^2 (u_n - 1), & n < 0, \end{cases} \quad (\text{A.1})$$

while the boundary conditions remain the same as in the dynamic case

$$u_n \rightarrow \begin{cases} \sigma, & n \rightarrow +\infty, \\ 1 + \frac{\Omega_0^2}{\Omega_1^2} \sigma, & n \rightarrow -\infty. \end{cases} \quad (\text{A.2})$$

For consistency we must also assume that

$$u_0^+ \leq \frac{1}{2}, \quad u_{-1}^- > \frac{1}{2}, \quad (\text{A.3})$$

where we are using notations:  $u_n = u_n^+$  when  $n \geq 0$  (phase 1) and  $u_n = u_n^-$  when  $n < 0$  (phase 2). The general solution for the finite-difference equations (A.1) takes the form

$$\begin{aligned} u_n^+ &= A_1 y_1^n + A_2 y_2^n + \sigma, \\ u_n^- &= B_1 z_1^n + B_2 z_2^n + 1 + \frac{\Omega_0^2}{\Omega_1^2} \sigma, \end{aligned} \quad (\text{A.4})$$

where

$$\begin{aligned} y_{1,2} &= 1 + \frac{\Omega_0^2}{2} \pm \frac{\Omega_0}{2} \sqrt{4 + \Omega_0^2}, \quad y_1 > 1, \\ z_{1,2} &= 1 + \frac{\Omega_1^2}{2} \pm \frac{\Omega_1}{2} \sqrt{4 + \Omega_1^2}, \quad z_1 > 1. \end{aligned} \quad (\text{A.5})$$

From (A.2) and the matching conditions  $u_0^+ = u_0^-$ ,  $u_{-1}^+ = u_{-1}^-$ , we obtain

$$\begin{aligned} u_n^+ &= \left(1 + \sigma \frac{\Omega_0^2 - \Omega_1^2}{\Omega_1^2}\right) \frac{y_2(1 - z_1)}{y_2 - z_1} y_2^n + \sigma, \quad n \geq 0, \\ u_n^- &= \left(1 + \sigma \frac{\Omega_0^2 - \Omega_1^2}{\Omega_1^2}\right) \frac{z_1(1 - y_2)}{y_2 - z_1} z_1^n + 1 + \frac{\Omega_0^2}{\Omega_1^2} \sigma, \quad n < 0. \end{aligned} \quad (\text{A.7})$$

Now, it is easy to check that the admissibility conditions (A.3) are satisfied only in the range

$$\sigma_p^- < \sigma < \sigma_p^+, \quad (\text{A.8})$$

where

$$\sigma_p^+ = \frac{\Omega_1^2}{2} \frac{z_1(1 - y_2) - y_2(z_1 - 1)}{\Omega_0^2 y_2(z_1 - 1) + \Omega_1^2 z_1(1 - y_2)},$$

$$\sigma_p^- = \frac{\Omega_1^2}{2} \frac{2 - (z_1 + y_2)}{\Omega_0^2(z_1 - 1) + \Omega_1^2(1 - y_2)}. \quad (\text{A.9})$$

Here  $\sigma_p^\pm$  represent the Peierls force, marking the limit of instability for the static solution; by substituting the appropriate values of  $y_2$  and  $z_1$  from (A.5) we obtain Eq. (46).

## References

- Abeyaratne, R., Knowles, J.K., 1997. On the kinetics of an austenite–martensite phase transformation induced by impact in a Cu–Al–Ni shape-memory alloy. *Acta. Mater.* 45, 1671–1683.
- Alshits, V.I., Indenbom, V.L., 1986. Mechanisms of dislocation drag. In: Nabarro, F.R.N. (Ed.), *Dislocations in Solids*. Elsevier, Amsterdam, pp. 43–111.
- Atkinson, W., Cabrera, N., 1965. Motion of a Frenkel–Kontorova dislocation in a one-dimensional crystal. *Phys. Rev.* 138 (3A), A763–A766.
- Braun, O., Kivshar, Y., 1998. Nonlinear dynamics of the Frenkel–Kontorova model. *Phys. Rep.* 306, 1–108.
- Carpio, A., Bonilla, L.L., 2003. Oscillatory wave fronts in chains of coupled nonlinear oscillators. *Phys. Rev. E* 67, 056621–056632.
- Cattuno, C., Costantini, G., Guidi, T., Marchesoni, F., 2001. Driven kinks in discrete chains: phonon damping. *Phys. Rev. E* 63, 046611.
- Currie, J.F., Trullinger, S.E., Bishop, A.R., Krumhansl, J.A., 1977. Numerical simulation of sine-Gordon soliton dynamics in the presence of perturbations. *Phys. Rev. B* 15, 5567.
- Earmme, Y.Y., Weiner, J.H., 1974. Breakdown phenomena in high-speed dislocations. *J. Appl. Phys.* 45 (2), 603–609.
- Earmme, Y.Y., Weiner, J.H., 1977. Dislocation dynamics in the modified Frenkel–Kontorova model. *J. Appl. Phys.* 48 (8), 3317–3331.
- Elmer, C.E., Van Vleck, E.S., 1999. Analysis and computations of travelling wave solutions of bi-stable differential difference equation. *Nonlinearity* 12, 771–798.
- Fath, G., 1988. Propagation failure of traveling waves in a discrete bi-stable medium. *Physica D* 116, 176–190.
- Fineberg, J., Marder, M., 1999. Instability in dynamic fracture. *Phys. Rep.* 313, 1–108.
- Freund, L.B., 1990. *Dynamic Fracture Mechanics*. Cambridge University Press, Cambridge.
- Gao, H., 1993. Surface roughening and branching instabilities in dynamic fracture. *J. Mech. Phys. Solids* 41, 457–486.
- Hirth, J.P., Lothe, J., 1972. *Theory of Dislocations*. McGraw-Hill, New York.
- Ishioka, S., 1973. Steady motion of a dislocation in a lattice. *J. Phys. Soc. Japan* 34 (2), 462–469.
- Johnston, W.G., Gilman, J.J., 1959. Dislocation velocities, dislocation densities, and plastic flow in lithium fluoride crystals. *J. Appl. Phys.* 30 (2), 129–143.
- Kessler, D.A., Levine, H., 2001. Nonlinear lattice model of viscoelastic mode III fracture. *Phys. Rev. E* 63, p. 016118/1–9.
- Kevrekidis, P., Weinstein, M., 2000. Dynamics of lattice kinks. *Phys. D* 142, 113–152.
- Kresse, O., 2002. Ph.D. Thesis, Department of Aerospace Engineering and Mechanics, University of Minnesota, pp. 1–200.
- Kresse, O., Truskinovsky, L., 2003. Mobility of lattice defects: discrete and continuum approaches. *J. Mech. Phys. Solids* 51 (7), 1305–1332.
- Langer, J.S., 1992. Models of crack propagation. *Phys. Rev. A* 46, 3123–3131.

- Langer, J.S., Lobkovsky, A.E., 1998. Critical examination of cohesive zone models in the theory of dynamic fracture. *J. Mech. Phys. Solids* 87, 1521–1526.
- Marder, M., Gross, S., 1995. Origin of crack tip instabilities. *J. Mech. Phys. Solids* 43 (1), 1–48.
- Marder, M., Liu, X., 1993. Instability in lattice fracture. *Phys. Rev. Lett.* 71, 2417–2420.
- Nabarro, F.R.N., 1987. *Theory of Crystal Dislocations*. Dover Publications, Inc., New York.
- Nishiyama, Z., 1978. *Martensitic Transformations*. Academic Press, New York.
- Noble, B., 1958. *Methods Based on the Wiener–Hopf Technique for the Solution of Partial Differential Equations*. Pergamon Press, New York.
- Pechenik, L., Levine, H., Kessler, D.A., 2002. Steady-state mode I cracks in a viscoelastic triangular lattice. *J. Mech. Phys. Solids* 50, 583–613.
- Peyrard, M., Kruskal, M.D., 1984. Kink dynamics in the highly discrete Sine-Gordon system. *Physica D* 14, 88–102.
- Rogula, D., 1967. Kinematic resonances in periodic structures. *Proc. Vibr. Problems, Warsaw* 3 (8), 215–237.
- Sharon, E., Gross, S.P., Fineberg, J., 1995. Local crack branching as a mechanism for instability in dynamic fracture. *Phys. Rev. Lett.* 74, 5146–5154.
- Slepyan, L.I., 1981. Dynamics of a crack in a lattice. *Dokl. Akad. Nauk SSSR* 258 (1–3), 561–564.
- Slepyan, L.I., 2000. Dynamic factor in impact, phase transition and fracture. *J. Mech. Phys. Solids* 48, 927–960.
- Slepyan, L.I., 2001a. Feeding and dissipative waves in fracture and phase transition. 1. Some 1D structures and a square-cell lattice. *J. Mech. Phys. Solids* 49, 469–511.
- Slepyan, L.I., 2001b. Feeding and dissipative waves in fracture and phase transition. 2. Phase-transition waves. *J. Mech. Phys. Solids* 49, 513–550.
- Slepyan, L.I., 2001c. Feeding and dissipative waves in fracture and phase transition. 3. Triangular-cell lattice. *J. Mech. Phys. Solids* 49, 2839–2875.
- Slepyan, L.I., 2002. *Models and Phenomena in Fracture Mechanics*. Springer, Berlin.
- Slepyan, L.I., Ayzenberg-Stepanenko, M.V., 2004. Localized transition waves in bi-stable-bond lattices. *J. Mech. Phys. Solids* 52 (7), 1447–1479.
- Slepyan, L.I., Troyankina, L.V., 1984. Fracture wave in a chain structure. *J. Appl. Mech. Tech. Phys.* 25 (6), 921–927.
- Thompson, R., 1986. The physics of fracture. *Solid State Phys.* 39, 1–129.
- Truskinovsky, L., 1996. Fracture as a phase transition. In: Batra, R.C., Beatty, M.F. (Eds.), *Contemporary Research in the Mechanics and Mathematics of Materials*. CIMNE, Barcelona, pp. 322–332.
- Truskinovsky, L., Vainchtein, A., 2003. Peierls–Nabarro landscape for martensitic phase transitions. *Phys. Rev. B* 67, 172103.
- Truskinovsky, L., Vainchtein, A., 2004. Explicit kinetic relation from “first principles”. In: Ogden, R., Gao, D. (Eds.), *Mechanics of Material Forces, Advances in Mechanics and Mathematics*. Kluwer, Dordrecht, 2003, pp. 1–8, in press.
- Weiner, J.H., 1964. Dislocation velocities in a linear chain. *Phys. Rev.* 136 (3A), A863–A868.
- Willis, C., El-Batanouny, M., Stancioff, P., 1986. Sine-Gordon kinks on a discrete lattice. Hamiltonian formalism. *Phys. Rev. B* 33 (3), 1904–1911.